The Effects of Marine Spectra and Temperatures on Photovoltaic Performance

Collin Krawczyk
College of Engineering, Informatics,
and Applied Sciences
Northern Arizona University
Flagstaff, Arizona 86011
Email: cak346@nau.edu

Michael Shafer
College of Engineering, Informatics,
and Applied Sciences
Northern Arizona University
Flagstaff, Arizona 86011
Email: michael.shafer@nau.edu

***Abstract*—Photovoltaic cells have been deployed in the marine environment in the past in order to assess performance at depth. Unfortunately, these applied studies have been somewhat limited in their scope due to the environmental conditions at the test location. In this paper, we present the results of silicon solar cell testing in a laboratory setting wherein the spectra produced by various water types are simulated over a wide range of depth and temperature. Spectra at depth were generated based on Bird's Clear Sky model and Jerlov's spectral absorption coefficients. These spectra were used in conjunction with a tunable solar simulator, source meter, and cold plate. This work discusses the spectra generation, experimental testing, and current-voltage curve parameters of silicon solar cells. Our results include short circuit current, open circuit voltage, and maximum power at ten different water types with depths up to 30 m. We highlight how the testing of silicon solar cells compare to previously published results and how depth and water quality impact subsurface power.**

***Index Terms*—Marine Telemetry, Solar Power, Modeling, Submerged, Irradiance, Biologging, Tag, Energy Harvesting, Photovoltaic.**

I. Introduction

Despite the potential for powering shallow sensors, wildlife tags, and autonomous underwater vehicles, solar power in the marine environment has seen limited research. Photovoltaic (PV) performance predictions are often modeled using the standard single-diode model, which predicts power well in most scenarios [1]. In the marine environment however, the light levels are often far below that for which the standard photovoltaic models are valid. In these scenarios, parameters such as series and shunt resistances can no longer be considered constant, leading to significant errors in power predictions under low light. As such, experimental cell testing is required to provide a full characterization of solar cell performance under various marine spectra and temperatures. This paper aims to provide a characterization of cell performance in the marine environment in order to expand our predictive capacity in a wide range of environmental conditions.

As early as the 1970's there was interest in how solar cells performed at depth [2]. While this early study reached depths up to 60 m, providing useful benchmarks for future work, this study was limited to the waters and environmental conditions of the testing location. Spectra, temperature, and irradiance levels were therefore all constrained. Other research has determined the spectral wavelength transmission through ocean water and has shown that wavelengths in the 300-400 nm and 600-700 nm ranges are absorbed as depth increases [3], [4], [5], [6].

While experimentation has provided a baseline for marine spectra and depth effects on photovoltaic performance, laboratory tests are limited. Some laboratory research has been conducted using both monocyrstalline and polycrystalline solar cells to determine IV characteristics in a more controlled environment [7]. This study considered various water types (deionized, artificial ocean, ocean, and lake) with depths up to 1 m. However, the power drop in this study appeared higher than in others' work. It was not clear that the authors had accounted for the solar simulator collimation angle and the effects that would have on cell irradiance. At the distances in the test, the reduction in irradiance would have been significant, given the 1-2° simulator collimation half angle. Regardless, the dearth of controlled testing of deep photovoltaic performance in the marine environment and the lack of low-light models highlight the need for this work.

In this paper, we have attempted to address both the issues constraining marine deployments of solar cell (irradiance, water type, temperature) and those constraining laboratory tests (depth). Rather than submerge cells, we simulate the marine spectra for various water types at various depths, testing the cells under a range of temperatures and using a tunable solar simulator to illuminate the cells. We present the results of this testing, highlighting how depth, water quality, and temperature affect cell performance.

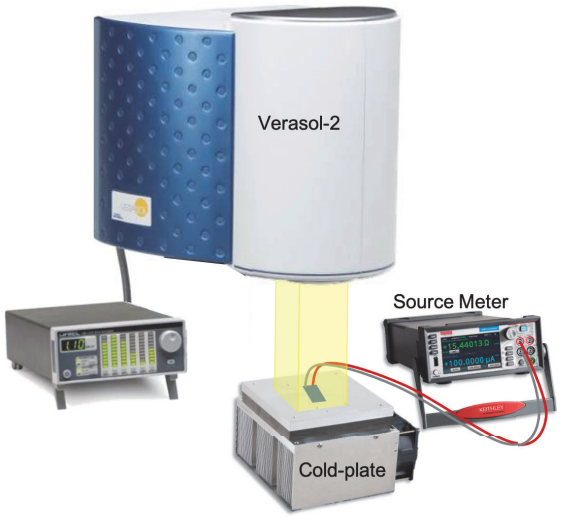

Fig. 1: Experimental setup with Verasol-2 illuminated temperature controlled PV cell. Blackout curtains (not shown) were wrapped around setup to reduce ambient light. To keep the solar cell temperature constant throughout testing, the cold plate's fans were kept outside of the blackout curtain environment.

II. Methods

A. Cell Temperature and Measurement

This study tested a IXYS SLMD600H10L monocrystalline silicon solar cell with published open circuit voltage, short circuit current, maximum power, and efficiency of 6.3 V, 25 mA, 111 mW, and 22%, respectively. The temperature of the cell was controlled by mounting it to a CP-121HT Peltier-Thermoelectric cold-plate. An image of the experimental setup is shown in Figure 1. The temperatures ranged from 0 - 30°C in 5°C increments. The temperatures of the PV cell on the cold-plate were verified to be within ±2°C over 0°C - 10°C temperatures and ±1°C over 15°C - 30°C temperatures using a FLIR A300 Series infrared camera (not show in the image). The current-voltage (IV) characterization of the cell at each test point was measured using a Keithley 2450 source-meter. These IV sweeps were performed between 0 - 7 V at 50 voltage steps in this range.

B. Spectrum Prediction

In order to test for a variety of water types and depths, spectra for both needed to be generated. Jerlov's 1976 characterization of downwelling spectra, which cataloged a range of water types or 'qualities', was used as a basis for spectral prediction at depth [8]. The water qualities range from Type I to Coastal Water 9 (CW9), where Type I is the clearest oceanic water and CW9 is the murkiest coastal water. Jerlov's classification of water qualities around the globe is shown in Figure 2. While the Jerlov characterization provided absorption coefficients, a surface spectrum was needed as an input to the water.

To determine the subsurface spectra, the SPCTRAL2 model described by Bird et al. was used to determine the global horizontal irradiance (GHI), direct normal irradiance (DNI), and diffuse horizontal irradiance (DHI) between 300 nm and 1100 nm wavelengths [9]. This model predicts the GHI, DNI, and DHI before crossing the air-water interface. The losses resulting from transmission through this boundary is accounted for in the transmitted GHI (TGHI) described by Hahn et al. [10]. This TGHI represents the initial spectrum just below the water surface. It is this spectrum that is affected by the aforementioned absorbtion coefficients to produce a total irradiance at depth (D) of

$$I(D) = \int \mathrm{TGHI}(\lambda)\, e^{-K_d(\lambda)D}\, \cos(\mathrm{PT})\, \mathrm{d}\lambda. \quad (1)$$

Here $K_d(\lambda)$ represent the water quality and wavelength specific absorption coefficient tabulated by Jerlov. The panel tile (PT) was assumed to be 0° with an assumed zenith angle of 0°, but deviation would only affect the magnitude of the irradiance rather than the shape of the spectrum. The effect of varying the magnitude of the input irradiance was accomplished by scaling the resulting spectra. This method of prediction was used to generate spectra of each of Jerlov's ten water qualities at depths from 0 to 30 m.

The subsurface spectral predictions for all water types at depths of 5 and 10 m are shown in Figure 3. This figure highlights how depth and water type affect the total irradiance, as well as the spectral shape at depth. It is this shape and the cell's spectral response that affect the light generated current in the cell, which is why, as Jenkins found, cell chemistries that under perform in terrestrial applications can outperform in the marine environment [3]. With spectral predictions made, they could be recreated using a tunable Verasol-2 solar simulator.

C. Spectrum Simulation

To simulate the variable spectra we used a Versol-2 LED solar simulator. This light source uses 21 LEDs each with narrow wavelengths in the band of 420 - 1050 nm to enable users to tailor the spectrum of the 2" x 2" output. This simulator allowed for custom spectra to be inputted at specific LED wavelengths. The LED setpoints were determined relative to the maximum spectral irradiance for each spectra. As an example, the spectrum predicted at 10 m in Type 1 water is show in

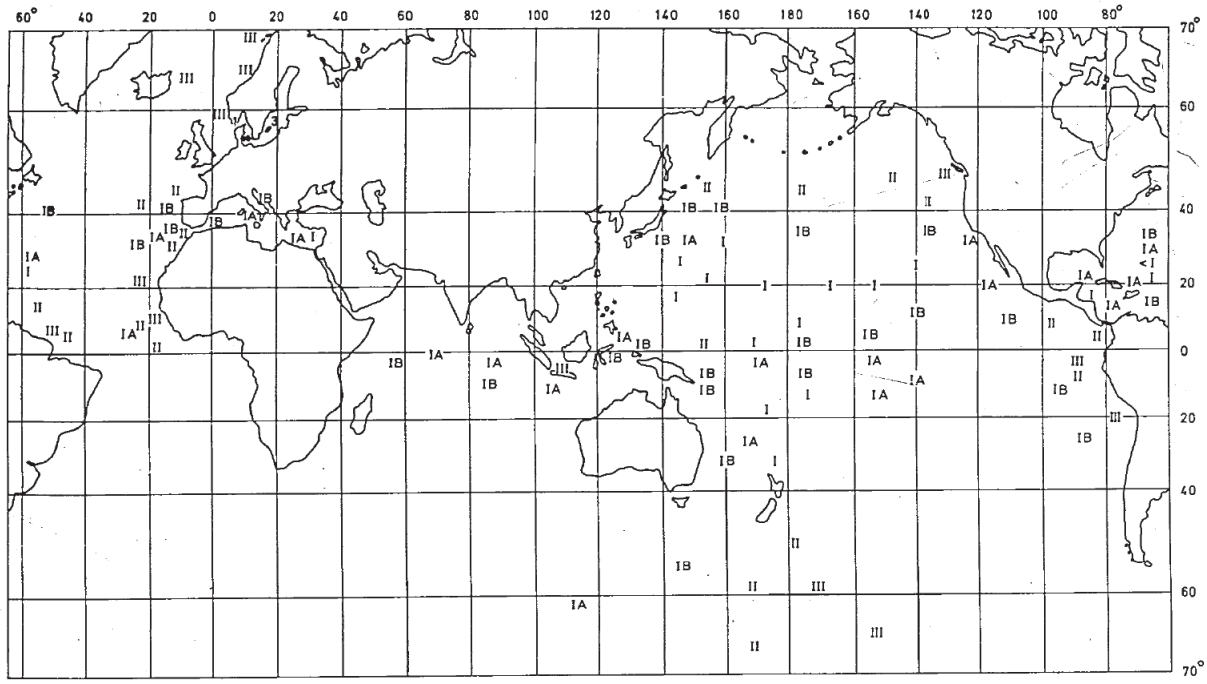

Fig. 2: Jerlov's classifications of global water qualities. Republished with permission of N.G. Jerlov, from Marine Optics, N.G. Jerlov, vol. 24, issue 3, 1976; permission conveyed through Copyright Clearance Center,Inc.

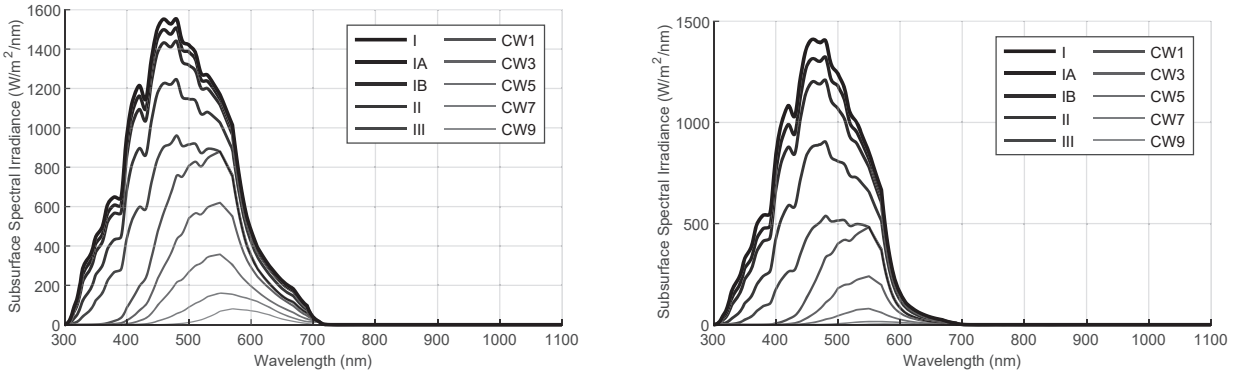

(a) Spectral Irradiance Spectra at 5 m

(b) Spectral Irradiance Spectra at 10 m

Fig. 3: (a) The subsurface spectra for all water qualities at 5 m (b) The subsurface spectra for all water qualities at 10 m. Notice how the 10 m spectrum for Type I water quality decreases substantially in the 600 - 700 nm range and how the overall maximum spectral irradiance decreases.

Figure 4. The LED setpoints are shown in this figure as red circles.

As seen in this Figure 4, a portion of the spectrum (<400 nm) could not be produced by the Verasol-2 because no LEDs included in the device emitted this wavelength. This is likely due to the fact that the spectral response for silicon cells and the irradiance in the clear-sky spectrum produce relatively little power in this band. Regardless, to account for this missing power in this test, all other LED power settings were increased slightly to account for the power in the spectrum below 400 nm. This accounting for missing radiative power may slightly over predict cell output power due to the shape of the SLMD600H10L's external quantum efficiency curve [10], but these errors will be quite small relative to the total power produced by the cell.

While the solar simulator was calibrated in the range of 100-1000 W/m^2, the total irradiance predicted at depth is often below the 100 W/m^2 level. In these cases, an MKS FSQ-ND10 neutral density filter (optical density

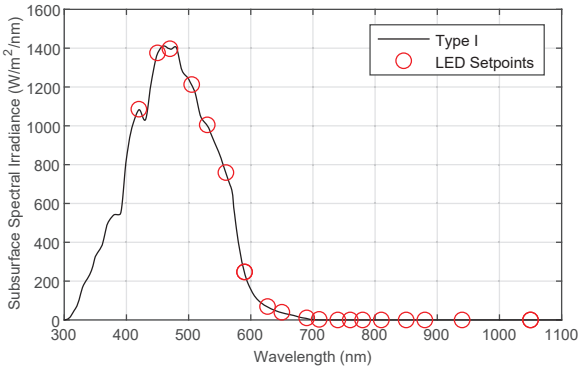

Fig. 4: The LED setpoints for a Type I water quality at 10 m. The setpoints are slightly higher than the spectra curve due to the addition of the irradiance within the 300 - 400 nm range.

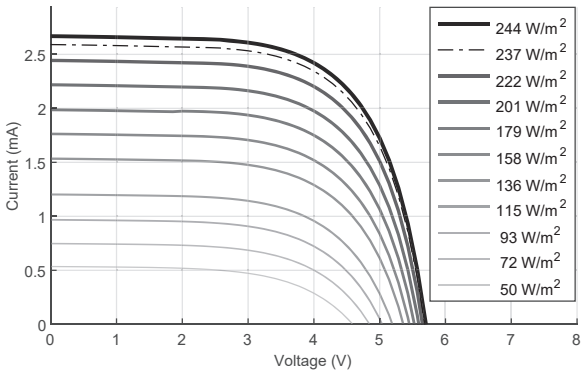

Fig. 5: IV Curves for Type I water quality at 10 m and 20 °C. Note that the nominal spectrum irradiance was 237 W/m^2. The final IV curve was taken at 244 W/m^2, slightly over the nominal but under the +25% extra irradiance limit.

of 1) was placed over the cell to keep the solar simulator in its calibrated range. In some cases of shallow depths and/or the most clear water types, the maximum output of individual LEDs in the Verasol-2 limited our ability to test the full radiative power predicted by equation 1. In these cases, the limiting LED was set to its maximum output power and the others were set to match the predicted spectral shape; The Versol-2 was able to match the spectrum but at a reduced total irradiance. Because these cases occurred only for high irradiance, the result from the reduced irradiance tests could then be extrapolated using standard PV modeling to predict the cell performance under the predicted irradiance. This method of extrapolation is further discussed in section III.

D. Testing Procedure

Due to the roughly 2,100 testing cases, an automated data collection method was necessary. To summarize, temperatures were tested between 0-30°C in 5°C steps, with 10 water types, and depths from 0-30 m in 1 m increments. The solar simulator and source meter were both connected to a desktop computer running a custom Matlab script which updated the spectrum for each test and then triggered and downloaded the IV data from the source meter. The temperature plate was manually adjusted for each temperature condition. For each of these cases, the irradiance below, and sometimes above, predicted by equation 1 were used in order to enable the aforementioned extrapolation and to enable predictions for TGHI lower than the prediction for a solar zenith of 0°.

While the Verasol-2 was calibrated down to 100 W/m^2, we found that the spectrum shape was valid down to 50 W/m^2 when outputted by the Verasol-2. This was verified using the Verasol-2 control panel and visually determining the irradiance at which the spectrum would retain its shape. Below 50 W/m^2, the spectrum would flatten. At every temperature, water type, and depth, the simulator would produce 10 irradiance steps starting at 50 W/m^2 up to the ending point. This ending point was defined as the maximum output power that the Verasol-2 could produce for a given spectrum or the nominal irradiance predicted by equation 1. To provide extra data points for use in future data processing, an extra +25% irradiance was added to the nominal irradiance, if possible. To simulate irradiances lower than 50 W/m^2, neutral density filters were added. With one neutral density filter, 10% of the simulated light would impact the solar cell. We were able to simulate irradiances between 5 and 50 W/m^2 with one MKS FSQ-ND10 neutral density filter and between 0.5 and 5 W/m^2 with two. The IV curves for a Type I water quality at 10 m and 20°C for all recorded irradiances is shown in Figure 5. The data set containing all IV curves categorized by water quality, temperature, irradiance, and depth can be found on our Zenodo [11].

E. Data Conditioning

For full solar cell characterization, the I_{SC}, V_{OC}, and the maximum power were calculated for each IV curve. The maximum power, I_{SC}, and V_{OC} were initially interpolated to determine results at the nominal irradiance of each spectrum at every depth and water type. In the cases when the simulator was unable to produce sufficient power, previously mentioned model-based extrapolation methods were used. This extrapolation was mainly used for high light levels where existing photovoltaic models are accurate. Approximately 20% of our data set was extrapolated using the forthcoming extrapolation methods.

Linear dependency of maximum power and I_{SC} on irradiance is predicted by models [12], and seen in our results (see Figures 6a and 6b). Therefore, linear extrapolation was used for these parameters. While these linear extrapolations are favorable for the I_{SC} and maximum power, the V_{OC} has a non-linear dependence on irradiance. This non-linear dependence takes the form of a natural logarithm [12]. This relationship between V_{OC} and irradiance can be approximated by

$$V_{oc} \approx V_{ocn} + \frac{nkT}{q} ln\left(\frac{E}{E_n}\right) \tag{2}$$

where V_{ocn} and E_n are the V_{OC} and irradiance under nominal conditions. The constants n, k, T, and q corresponds to the ideality factor, Boltzmann's constant, temperature, and electron charge, respectively. A non-linear fit method was introduced to implement this natural logarithm function to the V_{OC} data. An example fitting is shown in Figure 6c showing the close match between the model fit and the collected data.

III. Results

The V_{OC} is known to be the IV curve parameter most impacted by temperature [13]. While temperature does effect maximum power and I_{SC}, these parameters are impacted more by irradiance than temperature. To determine the temperature effects on maximum power, a comparison was made at 0 °C and 30 °C. The effects of temperature on maximum power is shown in Figure 7. Note that the lines of power in these figures are in the units of $\log_{10}$(mW/cm^2). For clearer water (near Type I), the maximum power was more impacted at deeper depths. There was nearly a 5 m shift in 1 mW/cm^2 for Type I at around 20 m. However, the temperature effects become minimal as the water becomes murkier. This is most likely due to the decrease in dependence on temperature and the increase in dependence on irradiance.

To determine effects of water quality and depth on the IV curve parameters, the temperature effects were averaged. At each depth and water quality, the IV curve parameters at each temperature were determined. This resulted in seven I_{SC}s, V_{OC}s, and maximum powers for every depth and water quality. These seven parameters were then averaged to obtain a singular data point for all depths up to 30 m and every water quality. The effects of water quality and depth on I_{SC}, V_{OC}, and maximum power are shown in Figure 8.

As expected, it was found that the water quality heavily impacts the I_{SC}, V_{OC}, and maximum power. At 20 m, Type I water had around 1 mW/cm^2 of power. For the same depth, Type CW9 water had around 1 x 10^{-5} mW/cm^2, five orders of magnitude different. While the water quality effects are immense at deeper depths, they are smaller are shallow depths. These effects are

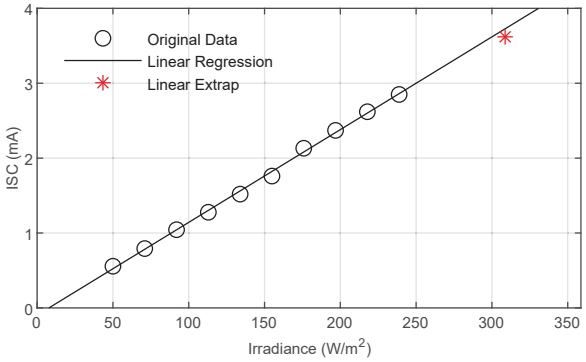

(a)

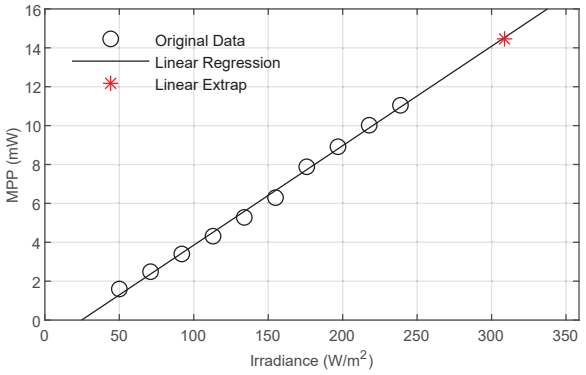

(b)

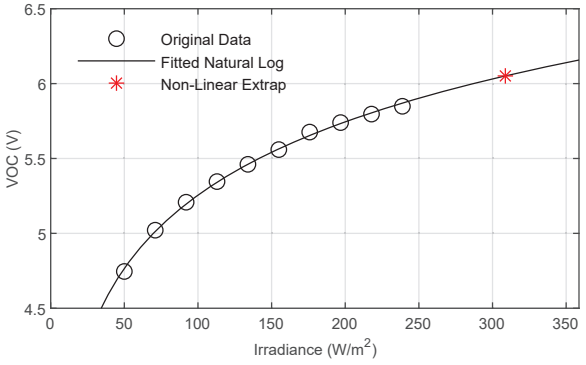

(c)

Fig. 6: Example data, curve fits, and extrapolations for (a) I_{SC}, (b) maximum power, and (c) V_{OC}. Note the linear shape of both I_{SC} and maximum power while V_{OC} is non-linear. The above figures were produced for Type I water at 10 m and 20 °C. The points of intersection were taken at the nominal irradiance of the spectrum.

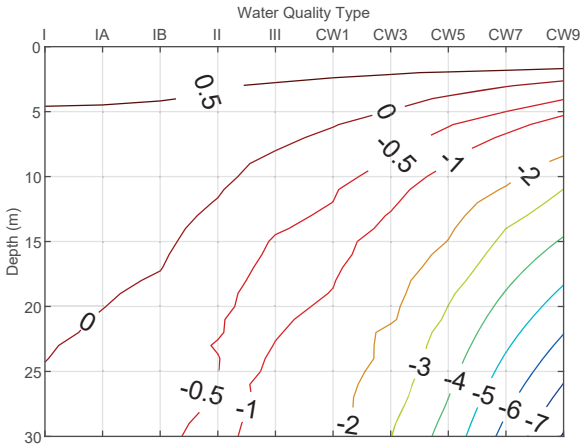

(a)

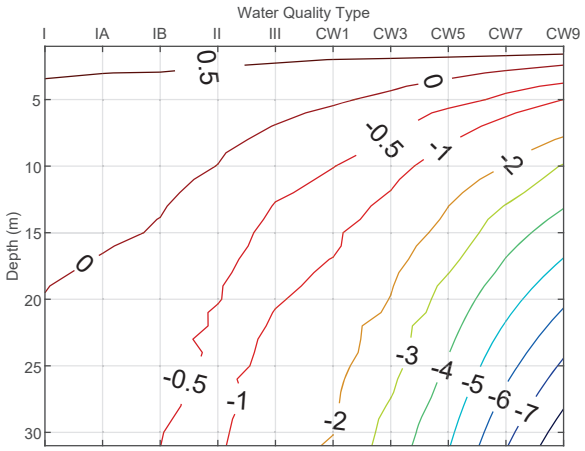

(b)

Fig. 7: Maximum power in $\log_{10}(\text{mW/cm}^2)$ at (a) 0°C, (b) 30°C as a function of depth and water quality. Note that for the maximum power, each band of constant power corresponds to a logarithmic decrease in power (e.g. line 0 corresponds to 10^0 mW/cm^2, line -1 corresponds to 10^{-1} mW/cm^2, etc...).

similar for I_{SC}. While the maximum power and I_{SC} had steep drop-offs as depth increased and the water quality became murkier, the V_{OC} had an almost linear decrease in voltage as depth increased. These linear decreases became steeper as the water quality became murkier.

To compare our results to previously published research, we calculated the effective efficiency at the maximum power points in our data, as well as those of previously reported work. The effective efficiency was defined as the maximum power normalized by the nominal irradiance at the surface, and provides a measure of how depth and water quality affect cell performance.

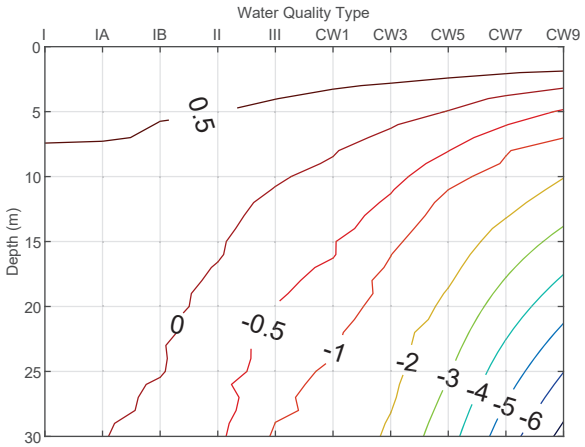

(a)

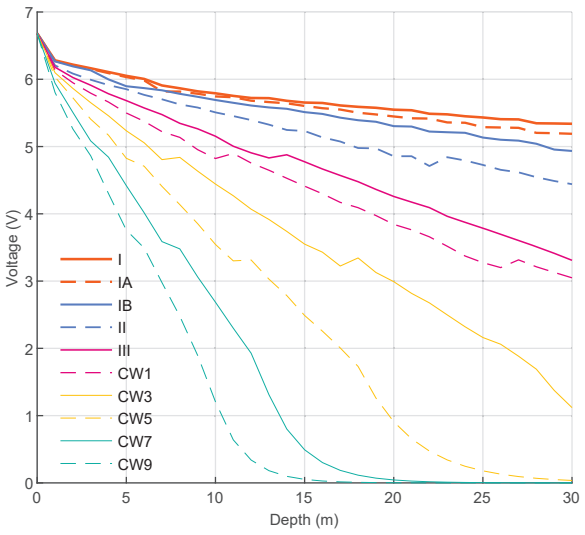

(b)

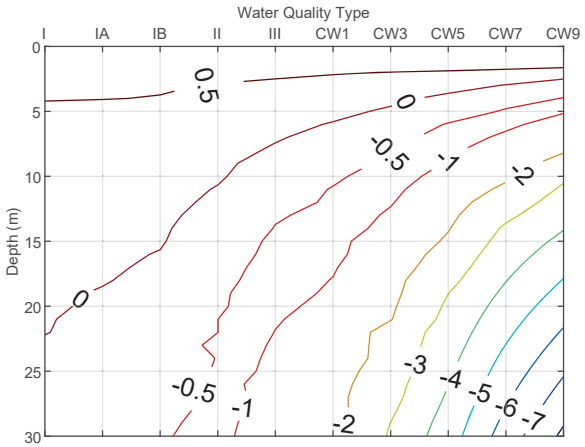

(c)

Fig. 8: The water quality and depth effects for the (a) I_{SC} in $\log_{10}(\text{mA})$, (b) V_{OC}, and (c) maximum power in $\log_{10}(\text{mW/cm}^2)$. Note that (a) and (c) are log plots where line 0 corresponds to 10^0 mA or mW/cm^2, respectively. The small jumps in (b) are caused by neutral density filter transition points.

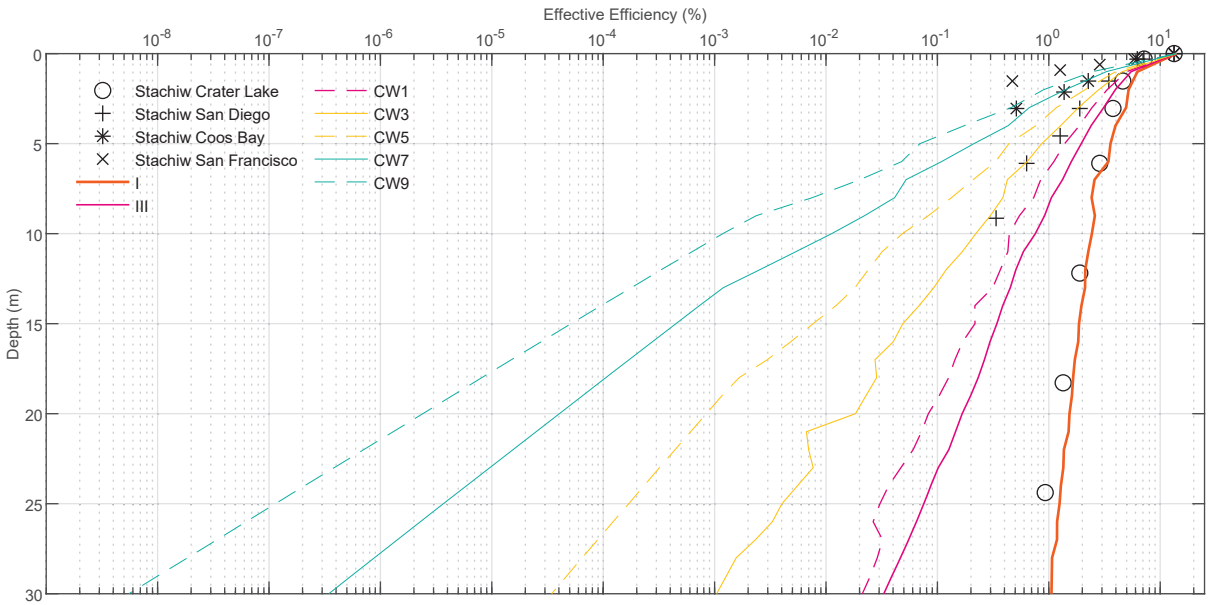

Fig. 9: Comparison between Stachiw's experimental testing data and our solar cell characterization. Several water types were omitted due to similar effective efficiencies to other water types. The Jenkin's data is omitted due to similar results to Stachiw's San Diego data set.

TABLE I: Decrease in efficiency every 10 m for each water quality.

	Water Quality									
	I	IA	IB	II	III	CW1	CW3	CW5	CW7	CW9
10 m Decrease (%)	61.3	64.3	67.6	76.5	87.4	92.0	95.8	99.1	99.8	99.9

Two data sets have been considered the standard for solar cell characterization in the marine environment. Stachiw's 1979 research characterized solar cells at various locations and at various depths [2]. The testing locations included Crater Lake, OR; Pacific Ocean in San Diego; Coos Bay, OR; and San Francisco Bay, CA. Additionally, Jenkins et al. characterized two solar cells at various depths in Key West, Florida, USA [3]. Power data from both data sets were extracted and the effective efficiencies were determined. Only Stachiw's data set is presented due to the similarities in the effective efficiencies between the Jenkin's data and Stachiw's San Diego data. The comparison between Stachiw's data and our data for various water qualities over depth is shown in Figure 9.

At the surface, we saw a nearly 14% effective efficiency. While the manufacturer states a 22% solar cell efficiency, the rated maximum power would suggest a maximum efficiency closer to 18%, which aligns closely with several other manufacturer specifications for monocrystalline silicon cells [14]. This is above the 14% calculated from the measured power and cell irradiance during the test. This 14% was calculated using Bird's Clear Sky model spectrum at 0 m. Using the AM 1.5G spectrum, an efficiency of 16.5% was found, closer to the 18%. When compared to calibration methods used by the Verasol-2 solar simulator manufacturers, an efficiency of roughly 14.5% was found for a monocrystalline silicon cell [15]. While our efficiency did not match the manufacturer's specifications, we are similar to calibrated monocrystalline silicon cells.

While most of Stachiw's data could be characterized by our results, Stachiw's San Francisco fell well below our lowest water quality. This means that the water quality in the San Francisco Bay is extremely murky, and the water qualities characterized by Jerlov do not go into this region. Based upon our results, a characterization of Stachiw's recording locations by water type could be determined.

IV. Discussion and Conclusion

Spectra generation using Bird's Clear Sky model in conjunction with Jerlov's absorption coefficients proved crucial in silicon solar cell characterization. These spectra allowed us to determine LED setpoints that were in-

put into a solar simulator. This solar simulator combined with a cold plate and source meter provided IV curves at ten different water types, temperatures up to 30°C, and depths up to 30 m.

While the impact of irradiance changes from depth and/or water quality are more significant, temperature does have a considerable affect on I_{SC} and maximum power. For example, Figure 7 shows that the cells in arctic waters could be deployed 2-5 m deeper than those in the equatorial latitudes where water temperatures are higher, while expecting similar levels of power output (assuming similar water qualities). This is especially true for the the oceanic water types.

The combination of both depth and water type heavily impact the amount of subsurface power available. In Type I water, there is nearly 1 mW/cm^2 of power at 20 m. This level of power is achieved in only 3 m of water for Coastal Water 9. Within the first meter, there is a significant drop in power for all water types. For water qualities Type I to CW3 where there is roughly 7 mW/cm^2 at the surface, the power drops to roughly 4 mW/cm^2 at 1 m and down to 2 mW/cm^2 for CW9. As the depth increases, the power drops almost exponentially with the exponential decay increasing as the water quality becomes murkier. These results are consistent with previously published subsurface solar cell response [2], [3], [5].

Summarizing these decreases in power output and relating to the power at the surface allows for the effective efficiency results of Figure 9. When viewed in this way, the effects of water quality and depth can be thought of as simply decreasing the surface efficiency of the silicon cell. We can see in Figure 9, that for oceanic water types I-III, a cell might expect approximately one order of magnitude change in efficiency at 10 m. After the first meter, all water types show a constant exponential decay in their efficiency with depth. For example, after the first meter the efficiency in Type I water could be modeled as $\eta(d) = \eta(2m)10^{-0.041(d-2m)}$, where d is the depth in meters. In this equation, the -0.041 relates to the slope of the lines shown in Figure 9, unique to each water type. The percent decrease in efficiency could be modeled as $\eta_{decrease}(\Delta d) = 1 - 10^{m\Delta d}$ where m is the slope of the exponential decay and Δd is the change in depth. By using a change in depth of 10 m, an approximate decrease in efficiency every 10 m could be determined. For Type I water, this corresponds to a decrease in efficiency of about 60% every 10 m. This 10 m decrease in efficiency for all water qualities is shown in Table I.

As expected, Type I water experiences the least amount of efficiency decrease every 10 m. This is due to Type I water being the clearest water while CW9 is the murkiest water. Every 10 m decrease can be modeled as $\eta_{decrease}(\Delta 10)^n$ where $\eta_{decrease}(\Delta 10)$ is shown in Table I and n is the number of 10 m steps taken (i.e. 20 m is two 10 m steps and 30 m is three 10 m steps). An estimated 20 m efficiency for Type I water can be modeled by $(61.3)^2$, which results in 37.6% of the original efficiency.

Given the significant reduction in power requirements of microelectronics in the previous decades, even microwatts of power can be considered sufficient of small sensor systems. Estimates can be made by considering a surface irradiance along with Figure 9 used to estimate where harvestable power might be available. For example, if we consider surface irradiance of $\mathcal{O}(1000)$W/m^2, Fig. 9 suggests that CW3 water could produce ~ 0.2 W/m^2 at a depth of 20 m and ~ 2 W/m^2 at a depth of 10 m. A small sensor system with a 3x3cm cell area would thus produce 18 μW at 20 m and 180 μW at 10 m.

When considering marine solar cell implementation, characterization of water quality may be necessary. Depending on water type, the amount of power available changes drastically. This drastic change demonstrates an operational depth difference between a water type of Type I at 20 m and water type Coastal Water 9 at 3 m. By considering the water type for deployment and power requirements of the solar cell, an operational depth can be determined for deployment.

ACKNOWLEDGMENT

This research was supported by the National Science Foundation (Grant No. 1537203).

REFERENCES

[1] W. De Soto, S. Klein, and W. Beckman, "Improvement and validation of a model for photovoltaic array performance," *Solar Energy*, vol. 80, no. 1, pp. 78–88, 2006. [Online]. Available: https://www.sciencedirect.com/science/article/pii/S0038092X05002410

[2] J. Stachiw, "Performance of photovoltaic cells in undersea environment," *Journal of Manufacturing Science and Engineering*, vol. 102, no. 1, pp. 51–59, 1980.

[3] P. P. Jenkins, S. Messenger, K. M. Trautz, S. I. Maximenko, D. Goldstein, D. Scheiman, R. Hoheisel, and R. J. Walters, "High-bandgap solar cells for underwater photovoltaic applications," *Photovoltaics, IEEE Journal of*, vol. 4, no. 1, pp. 202–207, 2014.

[4] J. Muaddi and M. Jamal, "Solar spectrum at depth in water," *Renewable Energy*, vol. 1, no. 1, pp. 31 – 35, Jul. 1991.

[5] ——, "Spectral response and efficiency of a silicon solar cell below water surface," *Solar Energy*, vol. 49, no. 1, pp. 29–33, 1992. [Online]. Available: https://www.sciencedirect.com/science/article/pii/0038092X9290123R

[6] M. Stoddard and F. Incropera, "Distribution of solar radiation in natural waters under field conditions," *Solar Energy*, vol. 28, no. 5, pp. 425 – 432, 1982. [Online]. Available: http://www.sciencedirect.com/science/article/pii/0038092X82902626

[7] P. Enaganti, P. Dewedi, A. Srivastava, and S. Goel, "Study of solar irradiance and performance analysis of submerged monocrystalline and polycrystalline solar cells," *Progress in Photovoltaics Research and Applications*, pp. 1–11, 03 2020.

[8] N. G. Jerlov, *Marine optics*. Elsevier, 1976.

[9] R. E. Bird and C. Riordan, "Simple solar spectral model for direct and diffuse irradiance on horizontal and tilted planes at the earth's surface for cloudless atmospheres," *Journal of Climate and Applied Meteorology*, vol. 25, no. 1, pp. 87–97, 1986.

[10] G. G. Hahn, L. A. Adoram-Kershner, H. P. Cantin, and M. W. Shafer, "Assessing solar power for globally migrating marine and submarine systems," *IEEE Journal of Oceanic Engineering*, no. 99, pp. 1–14, 2018.

[11] C. Krawczyk, "dynamic-and-active-systems-lab/iv-curves: Experimental photovoltaic performance (v1.0)," *Zenodo*, 2021. [Online]. Available: https://zenodo.org/record/5199305

[12] M. Chegaar, A. Hamzaoui, A. Namoda, P. Petit, M. Aillerie, and A. Herguth, "Effect of illumination intensity on solar cells parameters," *Energy Procedia*, vol. 36, pp. 722–729, 2013, terraGreen 13 International Conference 2013 - Advancements in Renewable Energy and Clean Environment. [Online]. Available: https://www.sciencedirect.com/science/article/pii/S1876610213011703

[13] A. Maka and T. S. O'Donovan, "Effect of thermal load on performance parameters of solar concentrating photovoltaic: High-efficiency solar cells," *Energy and Built Environment*, 2021. [Online]. Available: https://www.sciencedirect.com/science/article/pii/S2666123321000118

[14] IXYS KOREA LTD, *IXOLAR™High Efficiency SolarMD*, March 2012, data Sheet. [Online]. Available: http://ixapps.ixys.com/DataSheet/SLMD600H10L-DATA-SHEET.pdf

[15] "Comparisons of iv curves between xenon lamp-based and led-based solar simulators," *Oriel Instruments*, 2015. [Online]. Available: https://www.newport.com/p/VeraSol-2